New Zealand Journal of Marine and Freshwater Research

ISSN: 0028-8330 (Print) 1175-8805 (Online) Journal homepage: https://www.tandfonline.com/loi/tnzm20

Wave hindcast for the New Zealand region: Nearshore validation and coastal wave climate

Richard M. Gorman , Karin R. Bryan & Andrew K. Laing

To cite this article: Richard M. Gorman , Karin R. Bryan & Andrew K. Laing (2003) Wave hindcast for the New Zealand region: Nearshore validation and coastal wave climate, New Zealand Journal of Marine and Freshwater Research, 37:3, 567-588, DOI: 10.1080/00288330.2003.9517190

To link to this article: https://doi.org/10.1080/00288330.2003.9517190

New Zealand Journal of Marine and Freshwater Research, 2003, Vol. 37: 567–588
0028–8330/03/3703–0567 $7.00

Wave hindcast for the New Zealand region: nearshore validation and coastal wave climate

RICHARD M. GORMAN
KARIN R. BRYAN*
National Institute of Water and Atmospheric Research Limited
P.O. Box 11 115
Hamilton, New Zealand
email: r.gorman@niwa.co.nz

ANDREW K. LAING
National Institute of Water and Atmospheric Research Limited
P.O. Box 14 901, Kilbirnie
Wellington, New Zealand

*Present address: Department of Earth Sciences, University of Waikato, Hamilton, New Zealand.

Abstract Historically, wave data coverage of New Zealand's coast has been poor, particularly for directional records. With very few data sets available of more than 1 year's duration, it has been difficult to establish accurate wave climatologies. To help fill in the gaps in our wave records, the wave generation model WAM (WAve Model) has been implemented over a domain covering the south-west Pacific and Southern Oceans. The model has been used to hindcast the generation and propagation of deep-water waves incident on the New Zealand coast over a 20-year period (1979–98), using winds from the European Centre for Medium-Range Weather Forecasts (ECMWF). The resulting synthetic climatology is expected to provide a valuable tool for researchers and coastal planners. The hindcasts were compared with data from wave buoy deployments at eight representative sites around the New Zealand coast. With appropriate interpolation and correction for the effects of limited fetch and sheltering by land, the hindcast was found to provide a satisfactory simulation of wave conditions at sites on exposed coasts. Regression between measured and hindcast significant heights at the four deep-water sites (100–120 m) achieved scatter indices (ratio of root mean square error to mean) averaging 0.28. At the four shallower sites (30–45 m), the corresponding scatter index averaged 0.49, indicating that for regions of complex coastal topography, deep-water spectra do not represent inshore conditions well. Wave spectra can be considerably modified by the processes of refraction and shoaling. To address these effects, nearshore wave transformations in the outer Hauraki Gulf were investigated using the shallow water model SWAN (Simulating WAves Nearshore), which was used to derive wave statistics at nearshore locations from deep-water wave spectra obtained from the hindcast. The simulations were validated using data from an inshore site in 30 m water depth at Mangawhai on the north-east coast of the North Island. Use of the nested model improved the agreement between model and measured significant wave height, decreasing the scatter index from 0.50 to 0.26. The suite of tools provided by the hindcast and localised, shallow water models can provide accurate new wave information for most of New Zealand's coastline.

Keywords wave modelling; wave buoy data; New Zealand regional wave hindcast; coastal wave climate; refraction modelling

INTRODUCTION

New Zealand has a long shoreline exposed to high-energy wave conditions from the Southern and Pacific Oceans and from the Tasman Sea. Waves contribute significantly to the physical processes acting on both natural and constructed coastal features at a variety of time scales, both through damage during intense storms and through steady

M02066; Published 5 August 2003
Received 23 August 2002; accepted 27 February 2003

action over longer terms. If we wish to understand and plan for the effects of waves at New Zealand's coasts we must first acquire an understanding of the historic occurrence and causes of wave events by assembling an accurate and extensive wave climatology. To be of maximum value, the duration of the wave records making up such a climatology should be long enough to capture mean seasonal cycles and interannual variability, e.g., multiple cycles of the El Niño/Southern Oscillation. We would also like the full extent of the coast to be represented, so that a reasonably accurate description of the wave climate can be given for any coastal site of interest. Finally, directional information is important for many applications, e.g., estimating longshore sediment transport, planning orientation of beach design projects, and building protective structures such as harbour walls and groynes.

Numerical modelling is at present the only feasible way of meeting all of these requirements. Historical records from *in situ* measurements, typically made with wave riding buoys, provide only patchy coverage at a few sites around the New Zealand coast, with long-term (>1 year) and directional data being especially limited (Pickrill & Mitchell 1979; Stanton 1992; Laing 1993). In recent years, satellite data have become available, and there are now nearly 15 years of wave heights from satellite radar altimeters (Laing 2000). This source does not, however, provide directional or frequency information, and is often of limited application to coastal waters as a result of the influence of land on the return signal.

Long-term records of wind data are more readily available than the corresponding wave records. From analysis of these data, wind fields can be derived with the aid of atmospheric modelling. It then becomes possible to use the wind fields to drive a long-term wave hindcast. Over the last 20 years there have been several such applications. For example, Günther et al. (1998) have produced a 40-year hindcast of the north-east Atlantic Ocean using United States Navy archived operational wind fields. Some global hindcasts, of more relevance for the New Zealand region, have also been carried out. These include a 15-year hindcast by Sterl et al. (1998) using reanalysis wind fields from the European Centre for Medium-Range Weather Forecasts (ECMWF) to drive a WAM (WAve Model) simulation and, more recently, a 40-year Global Reanalysis of Ocean Waves (GROW) hindcast (Cox & Swail 2001). In these instances, validation from buoy data is almost entirely limited to the Atlantic and Pacific Oceans north of the Equator. Where Southern Hemisphere validation data have been available, wave models typically show poorer performance in these comparisons than for sources north of the Equator. This is attributed to the low density of data sources feeding atmospheric models and analyses (Cox & Swail 2001). Hence, with New Zealand coastal applications in mind, it is valuable to provide a regional hindcast with validation from local data, building on previous work (Laing 1992,1993) in which a second-generation model was used to provide a short (5 month) hindcast as a pilot study for the New Zealand region.

To meet the need for a detailed wave climatology of the New Zealand region, we have implemented the WAM wave generation model (Hasselmann et al. 1988) on a grid covering the principal source regions for waves incident on the New Zealand coast. This model has been used to create a 20-year wave hindcast, making use of the available *in situ* data for verification. A preliminary version of this hindcast, at lower spatial resolution, has been established and tested previously (Gorman & Laing 2001), obtaining good agreement with data from wave buoys in the Bay of Plenty (Macky et al. 1995) and near Foveaux Strait. In this paper we describe a more detailed validation of the updated hindcast.

The focus of this paper is on nearshore wave conditions derived from the hindcast. A companion paper (Gorman et al. 2003) will describe deep-water open ocean climatology derived from the hindcast, and discuss seasonal, interannual, and longer-term variations in wind and wave conditions. Coastal wave conditions are of importance as the majority of applications of wave information are concentrated in shallow, often partly protected, coastal waters. Of course it is also important that the validation data are from buoys that are generally found close to the coast. The wave generation model necessarily encompasses an extensive ocean domain at relatively low spatial resolution. In travelling shoreward, the waves can be considerably modified by the processes of refraction and shoaling over seabed of varying depth, diffraction, reflection, and sheltering by land. The extent and nature of these processes are highly site-specific and to quantify them we require a combination of numerical modelling and analytic methods. In this paper, we describe the hindcast and the methods by which nearshore wave statistics are derived by nearshore modelling, and the improvements this makes to validations.

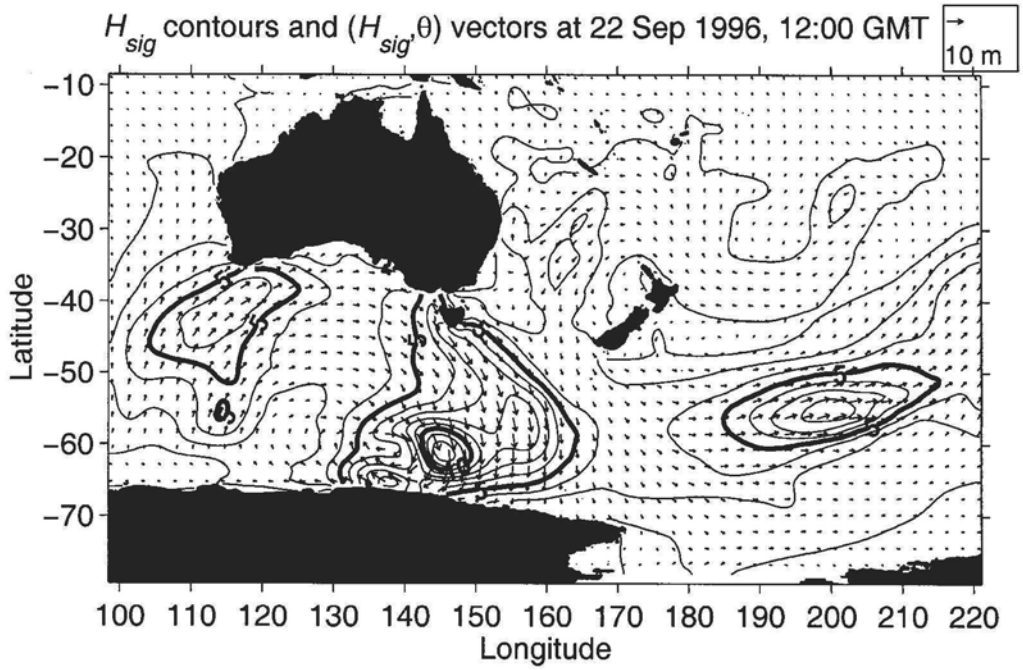

Fig. 1 Example output from the wave model, showing the distribution of wave height and direction over the 1.125° × 1.125° New Zealand regional grid, as hindcast for 12:00 Universal Time on 22 September 1996. Arrow length is proportional to wave height.

WAVE MODEL HINDCAST

The sea state at a given position (x, y) at time t can be described in a statistical way by a two-dimensional spectrum $F(f,\theta,x,y,t)$, which represents the energy density of the wave field as a function of wave frequency f and propagation direction θ. The WAM wave model (Hasselmann et al. 1988) describes the evolution of F using an action balance equation that accounts for the transfer of wave energy subject to the processes of generation by wind stress, propagation, four-wave weakly non-linear interactions, and dissipation by white-capping. In shallow water simulations, the additional processes of refraction by the seabed and/or currents as well as dissipation by bed friction can also be included, although in the present application of the WAM model we restrict our attention to deep-water processes. Each of the physical processes is explicitly incorporated in the model equations describing the evolution of the wave spectrum. As such, it is a third-generation model that, unlike first- and second-generation models, introduces no *a priori* assumptions on the shape of the energy density spectrum.

For hindcasting wave conditions in the New Zealand region, a rectangular grid was established covering latitudes 78.75°S–9°S and longitudes 99°E–220.5°E (139.5°W) at 1.125° resolution (Fig. 1). This region centres on New Zealand, extending westward beyond Australia's Indian Ocean coast, southward to the Antarctic, and incorporating the south-west Pacific Ocean. Energy density spectra were computed at 16 equally-spaced propagation directions and 25 logarithmically-spaced frequencies, between $f_1 = 0.0418$ Hz and $f_{25} = 0.4518$ Hz. At the spatial resolution used, depths <500 m are typically found no more than one cell from the coast. Refraction effects could not therefore be adequately resolved in the small fraction of the model domain where they might be significant, so a deep-water simulation was performed, neglecting refraction. The bathymetric data still required to locate "dry" cells, i.e., define land/ocean boundaries, were taken from the United States National Oceanic and Atmospheric Administration's ETOPO5 database (NOAA 1988), which provides global bathymetry at 5′ resolution. Wind data were sourced from the ECMWF reanalysis data set. This provides winds on a 1.125° latitude/longitude grid at 10 m elevation evaluated

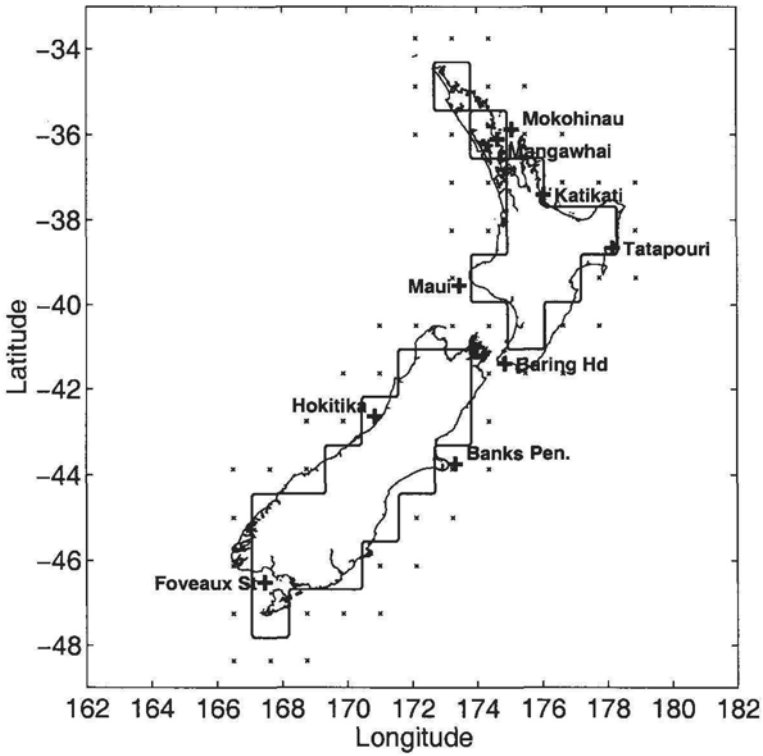

Fig. 2 Location map showing positions of wave buoys (+) used for comparison with the hindcast. The solid boundary indicates dry cells in the 1.125° × 1.125° New Zealand regional grid, whereas grid cells from which hindcast output spectra are interpolated are marked (×).

in a consistent way over the 15-year period 1979–93. The reanalysis was supplemented with archived ECMWF operational analyses to cover the following 5 years (1994–98). The potential for this change in data source to cause spurious apparent shifts in wind and wave climate is considered in the accompanying paper. It was found that although there is evidence of effects associated with changing resolution of tropical storm systems and of nearshore windfields, any biases in broader-scale wind fields are small relative to interannual variability. The data are provided at the analysis times of 00, 06, 12, and 18 h (Universal Time) on each day, between which the WAM model uses linear interpolation of wind speed and direction. The integration time step was set at 15 min for both propagation and source terms.

The model was then run for a 20-year hindcast of the years 1979–98 inclusive. Wave statistics over the entire grid were output at 3-h intervals. Full directional spectra were also archived at 3-h intervals from a set of 53 selected model cells, including all those adjacent to the New Zealand coast.

NEARSHORE WAVE STATISTICS

The modelling procedure described above provides a hindcast of deep-water wave conditions in the form of a full directional spectrum $F(f,\theta,x,y,t)$ at the centre of each wet 1.125° × 1.125° square in the grid. Since each model grid point represents the centre of a grid square which is either land or sea (dry or wet), the coastline in the model appears very "blocky" (see Fig. 2). For the study of coastal processes, we require wave conditions at various locations near the actual coastline, so the coast needs to be better resolved. Directional spectra that are interpolated directly from output in nearby model cells will poorly represent waves from directions where fetch is limited by the coastline. This can be improved by filtering to limit the spectral components from these directions to a magnitude consistent with the local wind speed and fetch, as described by Laing (1992).

In estimating the wave spectrum $F(f,\theta)$ at a point near the coast (e.g., point P in Fig. 3), a different treatment is applied to spectral components of waves depending on whether they propagate from seaward

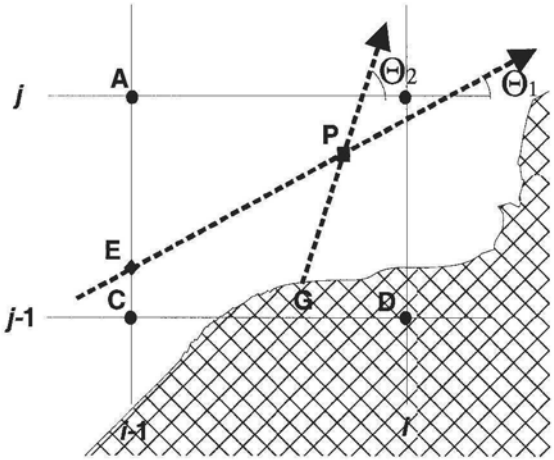

Fig. 3 Diagram illustrating the computation of spectral density $F(f,\theta)$ at the prediction point P. For propagation direction θ_1, for example, this uses an up-fetch spectrum at E, interpolated from hindcast spectra at cells A and C. For propagation direction θ_2, the fetch to the coast (PG) is used to compute a fetch-limited spectral density.

or landward directions. The fetch is first computed at 2° direction increments as simply the distance to the coastline. These distances are then averaged over the 22.5° direction bins of the model spectra while applying a $\cos\theta$ weighting to produce a mean fetch for each model propagation direction θ. The distance is also found in the up-fetch direction to the first crossing of a line between two wet grid points (e.g., point E on the line AC in Fig. 3). If this is less than the mean fetch to the coast, the spectral density at P is obtained by linear interpolation from the model values:

$$F(f,\theta,\mathbf{x}_P) = \left(\overline{EC}/\overline{AC}\right)F(f,\theta,\mathbf{x}_A) + \left(\overline{AE}/\overline{AC}\right)F(f,\theta,\mathbf{x}_C) \quad (1)$$

For directions in which it is the smaller of the two, the mean fetch to the coast (e.g., the distance $\overline{PG}$ in Fig. 3) is used with the local wind speed and direction to compute the empirical spectral density for that direction using the JONSWAP spectrum (Hasselmann et al. 1973), assuming a $\cos^2\theta$ directional distribution, i.e.,

$$F(f,\theta,\mathbf{x}_P) = F_J(f)D(\theta) \quad (2)$$

where the normalised directional distribution is taken as:

$$D(\theta) = \begin{cases} \frac{1}{\pi}\cos^2(\theta-\theta_{wind}), & |\theta-\theta_{wind}| < \pi/2 \\ 0, & |\theta-\theta_{wind}| \le \pi/2 \end{cases} \quad (3)$$

centred on the downwind direction θ_{wind}, and the JONSWAP spectrum is given by

$$F_J(f) = \frac{\alpha g^2}{(2\pi)^4 f^5} e^{-\frac{5}{4}(f_p/f)^4} \gamma^{\exp\left(-(f-f_p)^2/2\sigma^2 f_p^2\right)} \quad (4)$$

with gravitational acceleration g, a peak enhancement factor $\gamma = 3.3$ and a spectral width parameter:

$$\sigma = \begin{cases} 0.07, & f \le f_p \\ 0.09, & f > f_p \end{cases} \quad (5)$$

The peak frequency f_p and the energy-scaling factor α are derived from the fetch X and the wind speed U using fetch-limited growth formulae (Hasselmann et al. 1976):

$$\frac{f_p U}{g} = 2.84\chi^{-0.3} \quad (6)$$

$$\alpha = 0.0662\chi^{-0.2} \quad (7)$$

in terms of the nondimensional fetch parameter:

$$\chi = \frac{gX}{U^2} \quad (8)$$

These limited-fetch approximations were chosen by Hasselmann et al. (1976) to give a fetch-independent value of the shape parameter $\lambda = Ef_p^4/g^2\alpha$, as required for shape-invariance. Equation 6 lies within the envelope of subsequent fits to field data, as summarised, e.g., by Babanin & Soloviev (1998).

HINDCAST WAVE CONDITIONS AT BUOY SITES

A number of wave records are available from instruments deployed around the New Zealand coast during the hindcast period. We have selected nine deployments covering a variety of wave exposures (Fig. 2, Table 1). Wave statistics for the buoy sites were computed from the hindcast as described above. Occurrence statistics for significant height H_{sig}, mean direction θ_{mean}, and second moment mean period T_{m2} (defined in the Appendix) were computed over the full 20-year hindcast period. Significant height and mean period results were compared with data over the relevant deployment periods, as listed in Table 2 (directional data were not generally available). The wave climate hindcast at the buoy sites can be compared by reference to Fig. 5–7 which show occurrence distributions of significant wave

Table 1 Buoy deployments referred to in the validation of the wave model results. Columns describe the location, the deployment period from which data are available (notwithstanding any gaps in the records), the depth of deployment, whether directional (θ) data are available (✓) or not (×), and the funder/operators of the buoy (NIWA, National Institute of Water and Atmospheric Research).

Site	Latitude (deg.)	Longitude (deg.)	Data available	Depth (m)	θ	Funded/operated by
Foveaux Strait, Southland	–46.52083	167.45833	30 Apr 1989–30 Sep 1989	90	×	Electricorp/BTW Associates
Hokitika, west coast, South Island	–42.6405	170.8346	21 Sep 1996–30 Nov 1996	104	×	NIWA
Baring Head, Wellington	–41.4022	174.8467	21 Apr 1995–present	45	×	TranzRail, Wellington Regional Council, NIWA
Maui platform, Taranaki	–39.55	173.45	1 Sep 1976–30 Apr 1987	120	✓	Shell, BP, Todd Petroleum, Univ. of Auckland
Tatapouri, Gisborne	–38.6667	178.15333	5 Nov 1982–27 Sep 1984	39	×	Ministry of Works and Development
Katikati, Bay of Plenty	–37.4195	176.05397	1 Mar 1991–31 Dec 1995	34	✓	NIWA
Mokohinau I., Hauraki Gulf	–35.88333	175.0833	15 May 1998–present	100	✓	Auckland Regional Council
Mangawhai, Hauraki Gulf	–36.10808	174.64128	1 Sep 1996–30 Nov 1996	30	✓	NIWA
Banks Peninsula, Canterbury	–43.7558	173.3348	6 Feb 1999–present	76	✓	Environment Canterbury, Christchurch City Council, NIWA

height, mean period, and mean direction from the full 20-year simulation, as well as Table 3, which lists mean values and exceedence statistics for significant wave heights, as well as mean period and direction statistics.

South coast (Foveaux Strait)

In 1989–90, BTW Associates (on behalf of Electricorp NZ) moored a wave rider buoy in c. 90 m water depth to the west of Foveaux Strait (Fig. 2). A 153-day subset of significant height and mean frequency data from this record (May–September 1989) was used for comparison with the hindcast. The buoy data were first averaged over 3-h periods to match the model output cycle.

The model was able to closely match the main wave events in the study period (Fig. 4). Even 3-h averages of the measured values show somewhat more variation than the hindcast at short time scales. This is the result of the coarser 6-h resolution of the wind fields used in the hindcast. Over a 153-day comparison period there was a correlation of 0.79 between buoy and model H_{sig} estimates, with a bias (model–data) of -11 ± 8 cm (95% Confidence Level) and scatter index (root-mean-square error as a fraction of the mean) of 0.24 (Table 2). These verification results are similar to those obtained by Laing (1992), who applied a second-generation model over a similar region and, against about half of the same Foveaux Strait record used here, obtained a bias of –4 cm, correlation of 0.80 and scatter index of 0.25. This illustrates that the second generation approach of adjusting a near-universal spectral form can be successfully applied to wave generation by large-scale synoptic systems, as is the case in Southern Ocean waters where the more complex sea states resulting from rapidly changing wind fields are relatively infrequent.

There is evidence from comparisons with QuikSCAT data (Yuan 2002) that the upper range of wind speeds in the Southern Ocean are underestimated by the ECMWF reanalysis, which could be a cause of the negative bias in the hindcast wave height. The buoy record did not provide T_{m2} data, however the first moment mean frequency f_{mean} was available. The measured and hindcast averages of f_{mean} were 0.096 and 0.111 Hz respectively, with the comparison yielding a scatter index of 0.21 and a correlation of $R = 0.56$.

Exposure to the Southern Ocean makes the Southland-Fiordland coast the highest wave energy environment in New Zealand. The 20-year hindcast climate (Fig. 5) shows waves predominantly from

the south-west and west-south-west, although sheltering by Stewart Island has removed components from the south-east quadrant that would be evident further offshore. The distribution of hindcast H_{sig} (Fig. 6) has a tail extending well above the mean value of 2.66 m, with 3 m exceeded 29% of the time, and 5 m exceeded 5% of the time. The mean period T_{m2} has a narrower and more symmetric distribution (Fig. 7) than H_{sig}, and has a mean value of 8.27 s. Spectral peak periods are somewhat higher than T_{m2}, averaging 11.5 s.

West coast (Hokitika, Maui)

The next site we examine is off Hokitika, on the west coast of the South Island (Fig. 2), where 2 months of data were available from a 1996 wave buoy deployment. The hindcast for this period showed a 10% positive bias for both H_{sig} and T_{m2}. Model and data showed high correlation and relatively low scatter index, compared with other sites in Table 2.

The predominant wave direction in the 20-year hindcast climate (Fig. 5) is from the west-south-west, indicating a stronger influence from generation in the Southern Ocean than in the Tasman Sea, to which the site is fully exposed. Because of the high mountains of the Southern Alps running close to, and parallel to, the South Island west coast, local winds will tend to align with the coast. Hence local generation will also contribute to the high incidence of waves from the west-south-west. It might be suspected that with limited resolution of topography, the ECMWF wind fields might under-represent this orographic alignment, leaving an excessive onshore component in the winds that would in turn contribute to an overestimation of local wave generation. However Stanton (1998) compared ECMWF winds

Table 2 Comparison statistics for significant wave height (H_{sig}) and second-moment mean period (T_{m2}) measured and hindcast at the buoy sites. For both H_{sig} and T_{m2} the mean and standard deviation (σ) of the buoy data are followed by the bias (model-data mean) with 95% confidence levels, root-mean-square error (RMSE), scatter index (SI = RMSE/mean) and correlation coefficient (R) from the comparison of N records.

		H_{sig} data		H_{sig} model comparison				T_{m2} data		T_{m2} model comparison			
Site	N	Mean (m)	σ (m)	Bias (m)	RMSE (m)	SI	R	Mean (s)	σ (s)	Bias (s)	RMSE (s)	SI	R
Foveaux St	1114	2.60	0.98	–0.11±0.08	0.61	0.24	0.79						
Hokitika	486	1.97	0.87	0.22±0.11	0.49	0.25	0.87	6.87	1.13	0.66±0.14	1.04	0.15	0.72
Baring Hd*	55150	1.26	0.79	0.04±0.01	0.50	0.40	0.78	5.74	1.69	1.64±0.02	2.22	0.39	0.55
Maui*	19922	2.33	1.05	–0.42±0.02	0.84	0.36	0.72						
Tatapouri	6952	1.22	0.60	0.32±0.02	0.59	0.49	0.73	7.81	1.21	–0.47±0.04	1.21	0.16	0.56
Katikati	10292	0.81	0.53	–0.06±0.01	0.27	0.33	0.88	5.12	1.45	0.40±0.04	1.20	0.23	0.69
Mokohinau*	5376	1.38	0.88	–0.04±0.03	0.34	0.25	0.93	6.69	1.84	–1.20±0.07	1.65	0.25	0.82
Mangawhai	728	0.74	0.51	0.27±0.05	0.38	0.51	0.91	5.51	1.30	0.97±0.13	1.66	0.30	0.41

*Comparison period limited by the start or end of the hindcast (1 Jan 1979–31 Dec 1998).

Table 3 Long-term statistics for wave parameters derived from the hindcast at the buoy sites. Mean values are shown for significant wave height (H_{sig}) and second-moment mean period (T_{m2}), along with the sector of highest occurrence for mean wave direction. Percentage of H_{sig} records exceeding 3 and 5 m are also listed.

	H_{sig}			T_{m2}	
Site	Mean (m)	> 3 m (%)	> 5 m (%)	Mean (s)	Direction
Foveaux St	2.67	29	5.0	8.13	west-south-west
Hokitika	2.08	15	1.0	7.88	west-south-west
Baring Hd	1.23	2	0.10	7.10	south
Maui	1.97	10	0.55	6.97	west-south-west
Tatapouri	1.57	5	0.34	7.37	south
Katikati	0.86	1	0.04	5.75	east-north-east
Mokohinau	1.19	2	0.11	5.44	east-north-east
Banks Pen.	1.99	9	0.35	7.36	south-south-west

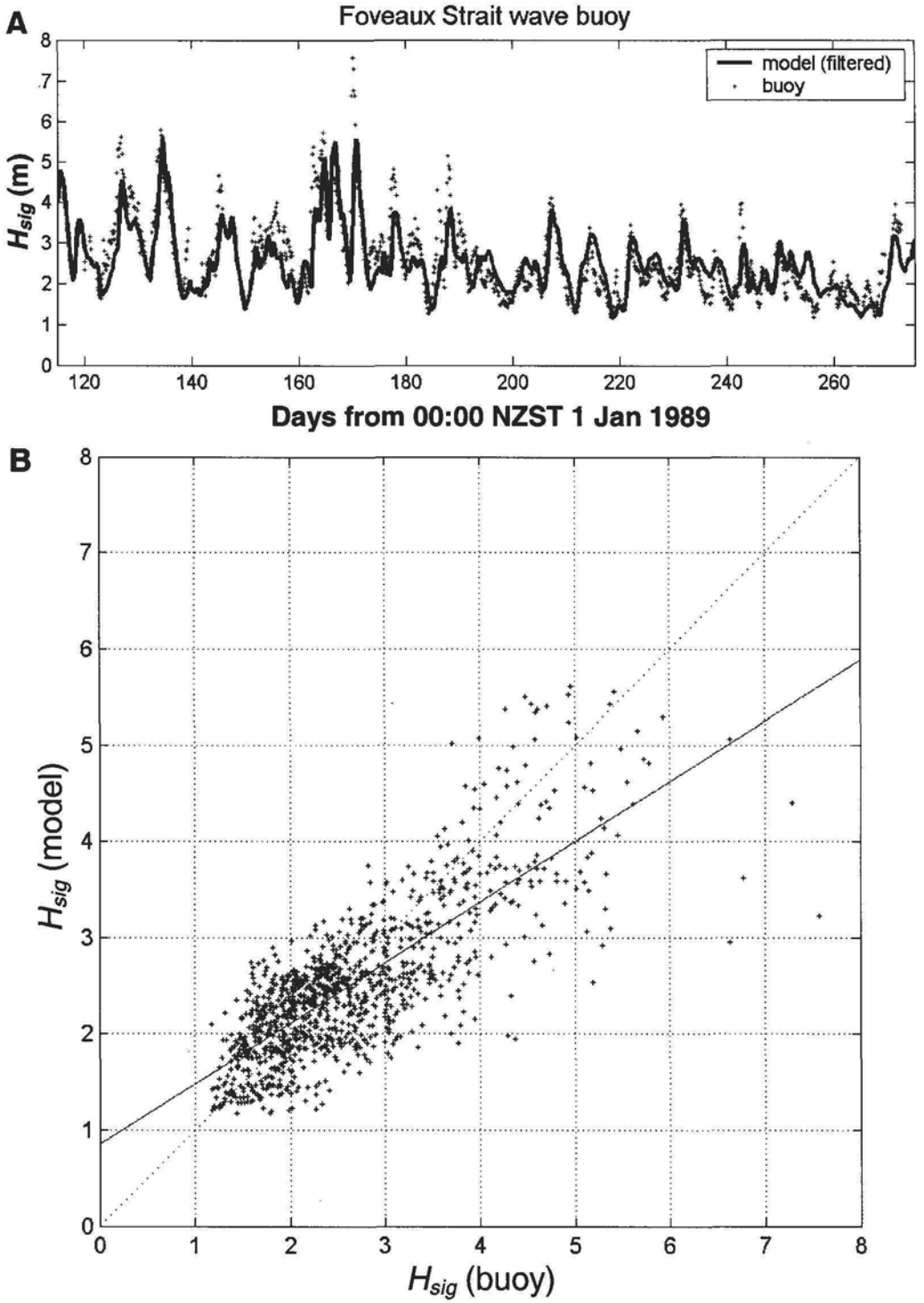

Fig. 4 Significant wave height at a wave buoy site near Foveaux Strait as simulated by the wave model and as measured by the buoy, shown as: **A**, time series; and **B**, regression, with the line of best fit and equivalence lines shown by solid and dashed lines respectively.

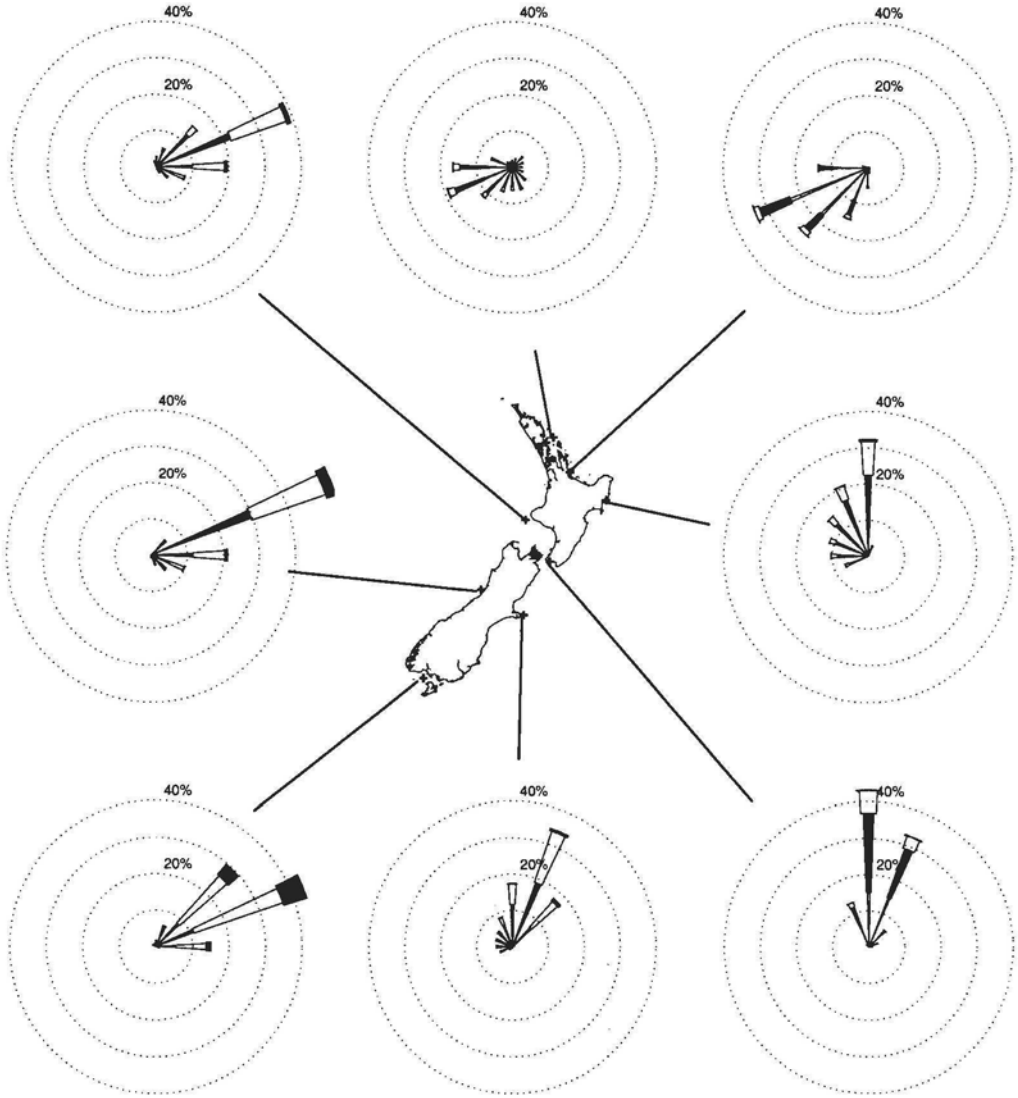

Fig. 5 Wave roses derived from the 20-year hindcast at eight wave buoy sites around New Zealand. Wave rose bars point in the direction TO which waves travel, and show occurrence of waves in height ranges 0–1 m, 1–2 m, 2–4 m, and >4 m (outermost).

with anemometer data from a 1994 buoy deployment off Hokitika, very close to the later wave buoy site, and found close agreement, with both sets of wind data showing a similar degree of longshore alignment.

The longest *in situ* wave record available in New Zealand comes from measurements made at the Maui-A platform off the Taranaki coast (Fig. 2) (Kibblewhite et al. 1982; Ewans & Kibblewhite 1990; Ewans 1998). In the 8 years (1979–86) of this record that we have used for model comparison, the hindcast underpredicts the measured significant height by 42 cm (Table 2). The model and data show a correlation index of $R = 0.72$, but with hindcast wave heights typically 80% of the measured values. As at Hokitika, wave conditions at the Maui site are dominated by swell from the south-west quadrant (Fig. 5) travelling up the South Island west coast

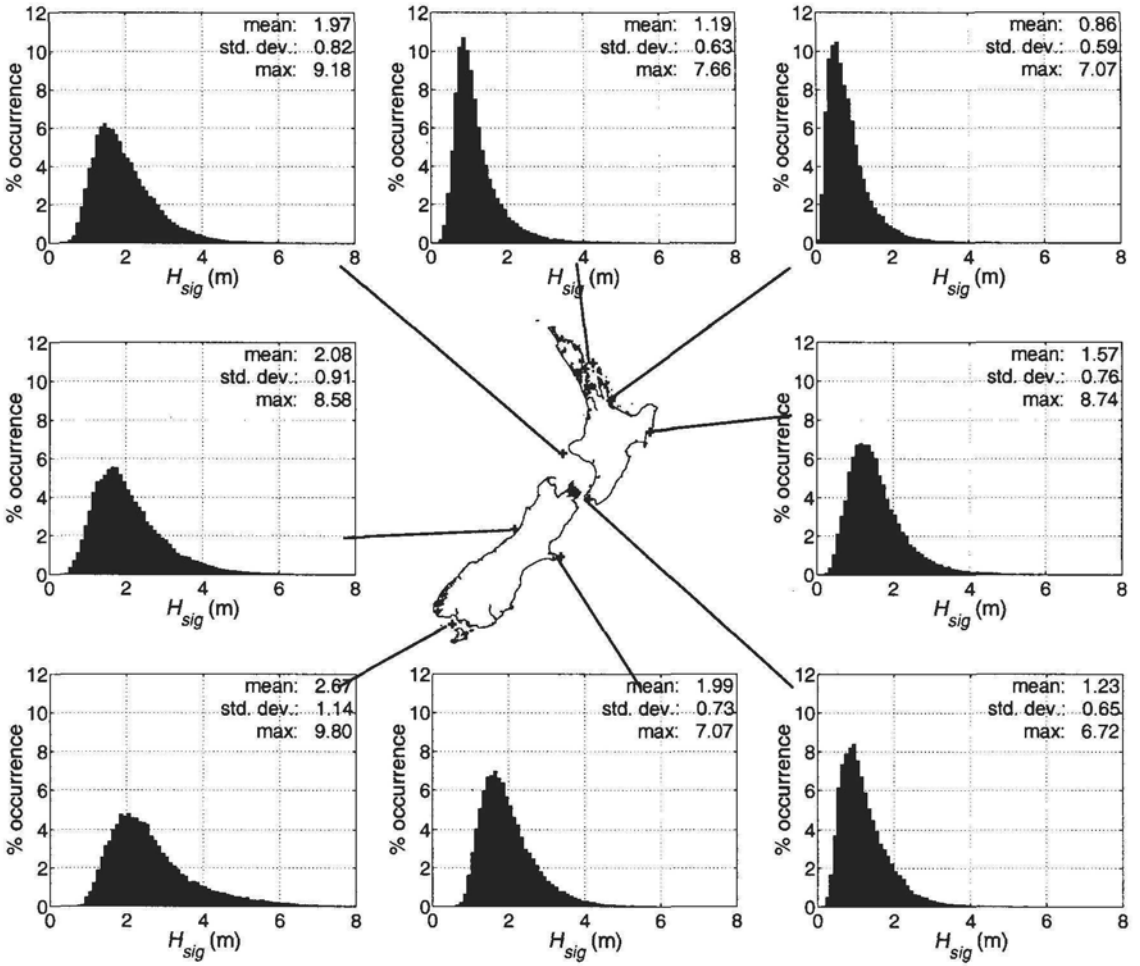

Fig. 6 Distributions of significant wave height derived from the 20-year hindcast at eight wave buoy sites around New Zealand.

from the southern Tasman Sea and beyond. It is curious to note that the measurements give a higher mean wave height for the Maui data than for the Hokitika record (albeit covering different time frames), whereas the hindcast gives lower mean H_{sig} at Maui than at Hokitika, both for the full 20-year record and for the respective data comparison periods.

In the model, wave energy from the dominant directions will be required to propagate diagonally past several cells of a coarsely represented land boundary, which raises the question of how accurately the model represents this process, given that the nominal land boundary is treated as absorbing. We shall return later to consider this effect in more detail.

The modelling procedure may also have several difficulties in adequately representing wave conditions at the Maui site produced by winds from the south-east quadrant. Wind records from the Maui platform show a high occurrence of strong south-easterlies, which comparisons with other records from the region show to be enhanced by a "channelling" effect through Cook Strait (Harris 1990). The ECMWF wind fields do show evidence of enhanced south-easterlies at the nearest grid cell, but with only two cells covering the greater Cook Strait region to the south-east (Fig. 2), the effect is likely to be inadequately represented in the wave model and in the procedure for interpolation and fetch correction described above. To isolate this effect, we have

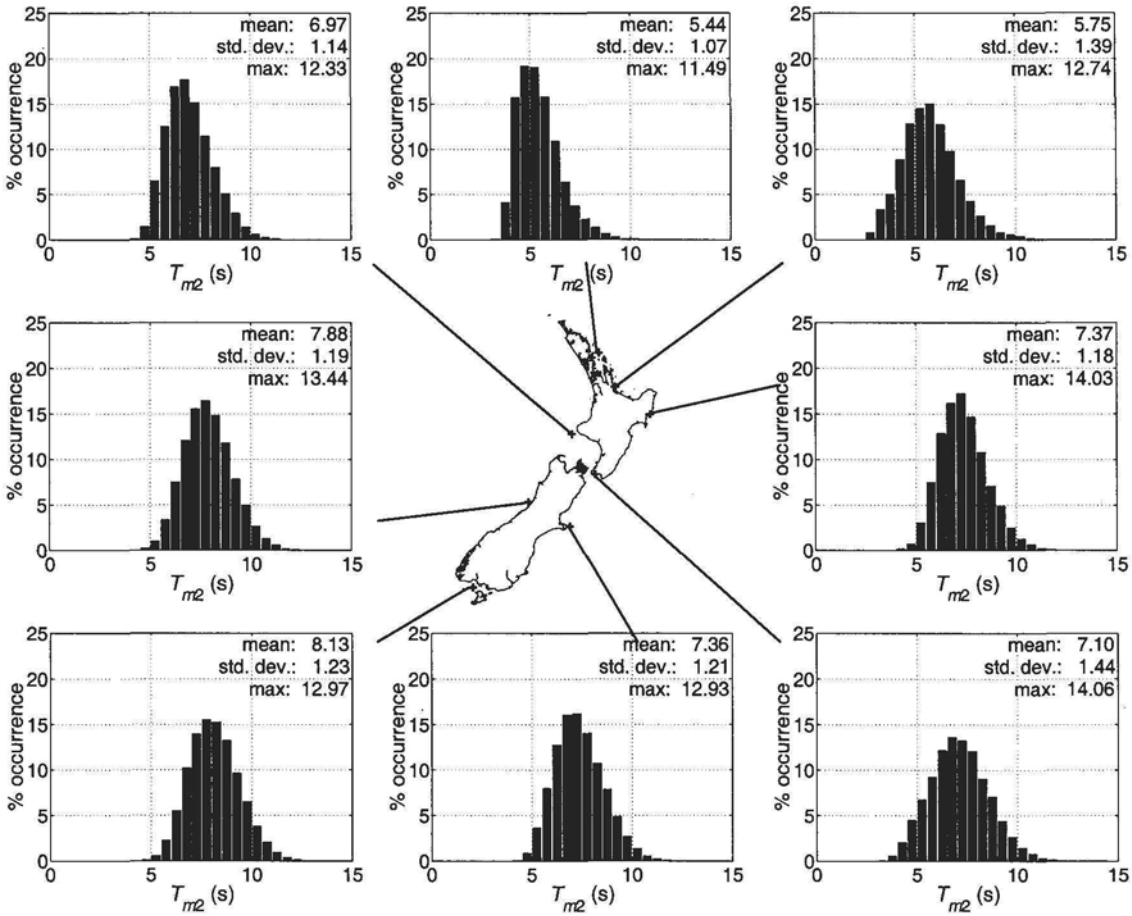

Fig. 7 Distributions of second-moment mean period derived from the 20-year hindcast at eight wave buoy sites around New Zealand.

partitioned the comparison period according to the direction of ECMWF winds at the cell nearest to Maui. We first compared hindcast significant height with data only for winds from the eastern and southern quadrants (i.e., from 45° through 225°, 33% of the record), which consist of short to moderate fetches across the greater Cook Strait region. The resulting model bias was –0.67 m, the scatter index was 0.43, and the regression coefficient was $R = 0.67$. For the remainder of the record, from the western and northern quadrants, we found bias = –0.29 m, scatter index = 0.31, and $R = 0.78$. It is evident that an underestimation of the wave energy generated by "channelled" local winds is detracting from the more satisfactory simulation of waves from the open sea.

East coast (Banks Peninsula, Baring Head, Tatapouri)

In 1999, a directional waverider buoy was deployed east of Banks Peninsula on the east coast of the South Island (Fig. 2) (Walsh & Mason 2000; Walsh 2001), in 76 m water depth. Although this was after the end of the hindcast period, preventing direct comparison, we include the hindcast results for this site so that the South Island east coast wave climate is represented.

Waves reaching Banks Peninsula predominantly arrive from the south-south-west (Fig. 5), indicating that generation in the Southern Ocean plays an important role, as it does for the other South Island sites, along with the influence of depressions to the

east, which frequently produce southerlies over considerable fetches directed towards the South Island east coast. Long-term mean values from the hindcast were T_{m2} = 7.53 s and H_{sig} = 1.97 m, whereas in subsequent data from the buoy (from February 1999 to the end of December 2001), the observed significant wave height (H_{sig}) averaged 2.1 m, while the zero-crossing wave period (T_z, approximately equivalent to T_{m2}) averaged 6.7 s.

In 1995 the National Institute of Water and Atmospheric Research (NIWA) moored a waverider buoy in 44 m of water off Baring Head, outside the entrance to Wellington Harbour (Fig. 2). The site is exposed to the south and south-east. The hindcast wave climate (Fig. 5) shows a predominance of waves from the south, indicating that the unobstructed fetches down the east coast of the South Island allow much of the swell seen further south to reach Baring Head. Mean periods showed a somewhat higher variance than was seen at Banks Peninsula, associated with a relatively larger contribution from local generation. The hindcast reproduced the recorded mean wave height with +4 cm bias, but a moderate level of agreement compared with other sites in terms of correlation (0.78) and scatter index (0.40). It has previously been noted (Laing 2001) that wave heights at this site often show unexpectedly rapid onset from local storms. Strong tidal currents affect the region, and local winds are influenced by the orography, features that may not be adequately resolved by the ECMWF wind fields. Thus, although the mean wave energy may be well represented by the hindcast, the details of storm events may not be fully reproduced.

At Tatapouri, on the North Island east coast, north of Gisborne (Fig. 2), data are available from a 2-year deployment in 1982–84 (G. Macky pers. comm.). The hindcast overestimates the wave height here, with a bias of 32 cm, scatter index of 0.49, and R = 0.73. The mean period, on the other hand, is underpredicted. The site is exposed from north-east through south, but southerly directions dominate the hindcast wave climate (Fig. 5). The buoy was deployed in 39 m, shallow enough that refraction effects need to be considered, particularly as the predominant wave direction is oblique to the coast (Fig. 5). In the first instance, hindcast spectra have been computed assuming water of infinite depth. If the coastline and all depth contours are straight, waves approaching the coast will refract and shoal in a simple way, and the above parameters can be re-evaluated for finite depth d by applying Snell's Law, which relates the change in wave angle to the change in group velocity, using conservation of energy flux. This is carried out by applying the transformations:

$$\theta \rightarrow \theta', S(f) \rightarrow S'(f) \quad (9)$$

where:

$$C_g(f,d)\sin(\theta'-\theta_{onshore}) = C_g(f,\infty)\sin(\theta-\theta_{onshore}) \quad (10)$$

$$C_g(f,d)S'(f) = C_g(f,\infty)S(f) \quad (11)$$

before computing wave spectral statistics. Here $C_g(f,d)$ represents the group velocity for waves of frequency f in water of depth d, whereas $\theta_{onshore}$ is the local shore-normal direction. Adjusting the hindcast estimates at Tatapouri in this way, we find some improvement in the agreement for significant wave height, with a model bias of +25 cm, scatter index of 0.44, and correlation R = 0.73. However such a simple treatment of nearshore effects is clearly insufficient to account for the discrepancy. It should be noted that there are extensive shoals (the Ariel Bank) lying some 13 km offshore. Depths of <10 m are found in these shoals (Gillbanks 1989), which can cause seas to break in heavy conditions. From the buoy site, these banks occupy c. 45° of arc from east to south-east, and can be expected to significantly affect the wave energy arriving from this sector.

North-east coast (Katikati, Mokohinau Islands, Mangawhai)

A comparison was made with data from a buoy deployed in 34 m water depth, 8 km offshore from the coast near Katikati in the Bay of Plenty (Fig. 2) during 1991–93 (Macky et al. 1995). There the correlation between hindcast and buoy wave heights was R = 0.88, and the mean bias was –6 cm (Table 2). The north-eastern coast of the North Island has a moderate wave climate (the mean significant height recorded off Katikati was 0.81 m), so the hindcast errors were relatively large compared to the mean, hence the scatter index for significant height was also relatively large (0.33).

The long-term wave climate shows predominantly onshore wave directions (Fig. 5), with the arc of the Bay of Plenty providing some limit to the range of exposure directions. There is a shadowing effect from Mayor Island, located 20 km offshore (Macky et al. 1995), but this only occupies 15° of arc and should be accounted for in the hindcast record by the fetch-limited filtering procedure described above. Combined with a bathymetry that has little longshore variation, this suggests that

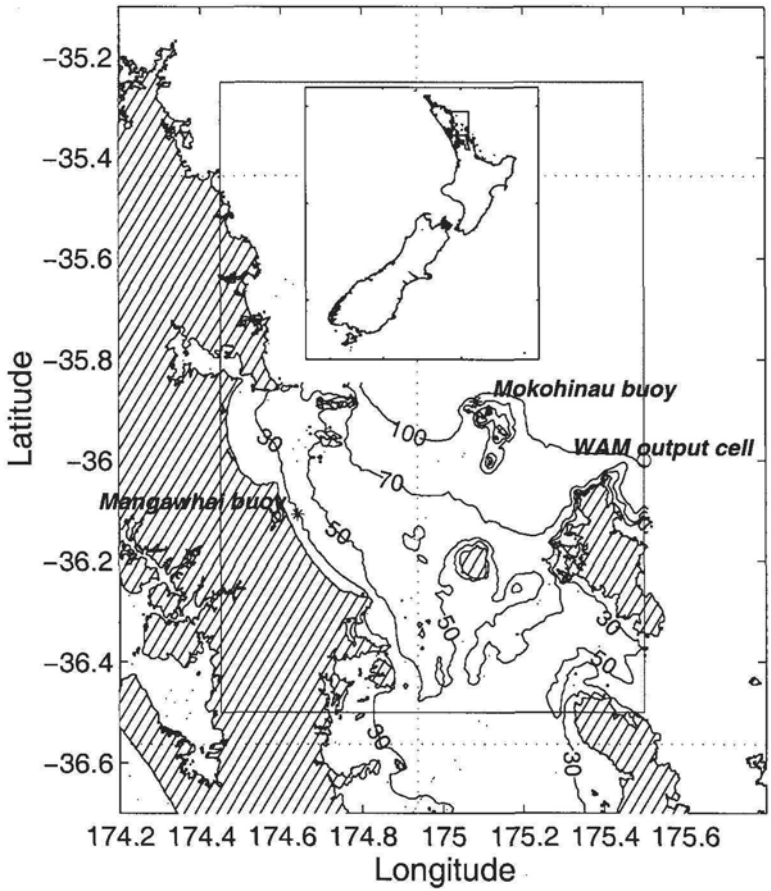

Fig. 8 Location map for the outer Hauraki Gulf, showing depth contours and the Mangawhai and Mokohinau Islands buoy sites. Dashed lines mark cell boundaries of the deep-water WAM grid. Deep water wave spectra from the cell marked (o) were used to provide boundary conditions for SWAN refraction modelling, carried out in the domain marked by the solid rectangle (and by the shaded rectangle in the inset New Zealand map).

refraction should have only a moderate effect on mean wave conditions. Indeed, when a "straight-coast" correction is applied to refract the hindcast in to buoy depth, the significant height bias is only slightly changed, to –9 cm, as are the correlation (0.87) and scatter index (0.34).

The distribution of wave heights (Fig. 6) is weighted to considerably lower values than at the sites further south described above. The distribution of mean period (Fig. 7) is also skewed, with a relatively high occurrence of short period (3–4 s) waves. This is indicative of a relatively greater contribution from local generation over moderate fetches than is seen further south.

In May 1998 the Auckland Regional Council deployed a directional waverider buoy in 100 m depth at a site north of the Mokohinau Islands in the outer Hauraki Gulf (Fig. 2). The model provided a close match to the 1998 data included in the hindcast period, with a bias of –4 cm, scatter index of 0.25, and $R = 0.93$. The mean period is underpredicted by 1.2 s, but the correlation of $R = 0.82$ is the highest of the sites examined.

This location is exposed to a similar wave climate to that observed at Katikati, though with a somewhat larger exposure arc, so waves from the north-east through east predominate (Fig. 5). There is also a noticeable representation of waves from the south-west, which is a predominant wind direction (along with north-easterlies). The fetch in the "shoreward" south-west direction is not negligible (c. 50 km), so this part of the hindcast wave climate will be moderated by the empirical "fetch-limited" spectral density (Equation 2), rather than by interpolated hindcast spectra (Equation 1).

The distribution of wave heights (Fig. 6) is also weighted to lower values, though to a lesser extent than at Katikati. The distribution of mean period (Fig. 7) is highly skewed at this site, with a sharp rise in occurrence around $T_{m2} = 4$ s.

A waverider buoy was deployed in 30 m of water off Mangawhai beach (Fig. 2), and inshore from the

Mokohinau Islands site, for 3 months of 1996. The results at the Mokohinau Islands buoy site show that the hindcast closely reproduces deep-water conditions in this region. However the Mangawhai site is affected by sheltering by headlands and several offshore islands (Fig. 8), which can be accounted for by the fetch-limited correction procedure described above, as well as by refraction and diffraction by the surrounding shoals and islands, which are not taken into account. Consequently, the hindcast heights show the largest positive bias (+27 cm) and highest scatter index (0.51) of the buoy comparisons. The high correlation (R = 0.91) is consistent with wave generation being adequately represented at source, but nearshore dissipation being poorly scaled. The mean period is also overpredicted (bias = +0.97 s).

If a straight-coast refraction correction is applied to the hindcast, the significant height bias and scatter index are reduced only slightly, to 22 cm and 0.44 respectively. As for the Tatapouri data, this correction cannot account for refraction by complex bathymetry offshore. To address this issue we require more detailed nearshore modelling methods, which we describe below.

Summary of the hindcast nearshore wave climate

The wave climate at any part of the coast is a result of generation by weather systems throughout the surrounding waters of the Pacific and Southern Oceans and the Tasman Sea, the transformation of the wave fields as they propagate, and the sheltering effects of land. The variation in wave climate around the New Zealand coast results from differences in the influence of these processes. First, the strongest winds in the region, on average, are located to the south of New Zealand, c. 60°S, where strong westerlies are prevalent. Waves reaching New Zealand from these source areas will largely arrive from southerly and westerly directions, and have relatively long periods as a result of the large propagation distances (up to thousands of kilometres).

In the mid latitudes directly affecting New Zealand, weather systems generally travel from west to east. These will result in wave energy arriving at all parts of the coast from a wide range of directions, but with some biases. For example, low pressure systems moving into waters east and south-east of New Zealand will tend to direct winds from the south through south-east towards the east coast. Also, some of the most intense storm conditions result from cyclones moving down from the tropics, but these are infrequent, and largely restricted to the summer months.

As a result of these influences, directional distributions (Fig. 5) are weighted to waves from southerly through westerly directions at all sites examined except for those on the north-east coast. The latter have a more uniform spread centred on the onshore direction. The peak of the wave height distributions (Fig. 6) shows a trend to shift from higher to lower values in moving up the country from the south-west to the north-east, with mean H_{sig} decreasing from 2.7 m in Foveaux Strait in the southwest, to 0.85 m at Katikati on the north-east coast. But the variation at the top end of the distributions is less marked, with the maximum H_{sig} of the 20-year hindcast only decreasing from 9.8 to 7.0 m between the two sites. Mean period distributions (Fig. 7) also show a trend from the south-west to the north-east. In the former instance, a symmetrical distribution is seen, resulting from waves arriving from generating systems at a variety of distances and intensities, meaning there is generally some at least moderate level of swell present. On the north-east coast, the distributions peak at lower values, and are skewed to have a rapid rise below the peak and a long tail above the peak. This indicates that there are frequent occasions when local generation of short waves (period c. 4 s) can dominate over a low level of swell energy.

NEARSHORE WAVE TRANSFORMATION MODELLING

SWAN model

Although WAM has been adapted for shallow-water effects, it uses an explicit numerical scheme for propagation, which is only stable if it tries to move wave energy somewhat less than a grid space in each time step. This means that for the high spatial resolution needed in coastal applications, an impracticably short time step is required. There is also the need to simulate other phenomena specific to nearshore applications such as depth-limited wave breaking and interactions with changing currents and tides. It is for such applications that models such as SWAN (Holthuijsen et al. 1993; Ris et al. 1994; Booij et al. 1999; Ris et al. 1999) have recently been developed.

SWAN is similar to WAM in that it is a third-generation spectral model based on a version of the radiative transport equation. The numerical schemes in SWAN (Ris et al. 1994) were developed from those used in the second-generation HISWA model (Holthuijsen et al. 1989). The discretised spectrum

is partitioned into four quadrants, and a sequence of four forward marching sweeps is used to propagate the waves of each quadrant with an upwind finite difference scheme. This cycle is carried out iteratively, to allow boundary conditions to be matched between quadrants and an equilibrium solution obtained.

The SWAN model uses similar source terms to WAM, accommodating the processes of wind generation, white-capping, bottom friction, and quadruplet wave-wave interactions. In addition it treats triad wave-wave interactions and depth-induced breaking (Ris et al. 1994). The white-capping term is derived from the model of Hasselmann (1974), which considers white-caps as randomly distributed pressure pulses. The dissipation coefficient for this formulation was assigned the value $C_{ds} = 2.36 \times 10^{-5}$ (Komen et al. 1984). The representation of wave energy dissipation at the seabed is based on the empirical JONSWAP form (Hasselmann et al. 1973), with a friction coefficient $C_{bottom} = 0.038\ m^2\ s^{-3}$.

In the present application, a rectilinear spatial grid with 750 m × 750 m cell sizes was defined covering the northern Hauraki Gulf out to the continental shelf (Fig. 8). Bathymetry was adapted from a 1.5 km × 1.5 km resolution grid developed in previous hydrodynamic modelling studies of the Hauraki Gulf (Greig & Proctor 1988; Black et al. 2000). In spectral space, 24 direction bins and 33 frequency bins were used (matching the WAM frequency bins but extending the upper limit to 0.802 Hz). The model was run in quasi-stationary mode, in which time-dependence is removed and a single equilibrium solution obtained by iteration.

Directional wave spectra were extracted from the nearest cell of the WAM hindcast, and applied along the entire northern and eastern offshore boundaries. As noted above, comparison with data from the Mokohinau Islands buoy indicates that the hindcast provides an accurate representation of deep-water wave conditions in this region. Wind input was ignored. Instead, SWAN propagated wave spectra shoreward from the boundaries without considering local wind-sea generation.

Comparison with Mangawhai data

Wave heights at the nearest cell of the deep-water model (Fig. 9, Table 4) are typically double those observed at the Mangawhai buoy. The discrepancy becomes particularly marked when waves reach the offshore site from the south-east quadrant, and are blocked from reaching Mangawhai by land (notably Great Barrier Island and the Coromandel Peninsula). When, as described earlier, we generated nearshore statistics by taking the hindcast spectra and filtering to allow for limited local fetches (Fig. 10, Table 4), the hindcast wave heights were reduced to values much closer to those measured. A similar level of agreement is maintained throughout the study period, including both high- and low-energy events. Some bias (+0.26 m) remains however, with a persistent overprediction of wave heights. This may partly result from the energy densities for fetch-limited directions being computed using ECMWF winds interpolated from the nearest offshore grid cells, without taking account of the typically lighter winds inshore where there is some local sheltering. Some improvement is also noted in the estimate of mean period. One example is seen in Fig. 10 c. 17–18 September, a time of low-energy, long-period wave activity, suggesting that minimal wind-sea was present as a result of a persistent offshore wind. Filtering removes spurious wind-sea generated in the hindcast, leaving longer-period swell to dominate.

Use of the SWAN model to refract offshore hindcast spectra in to shore results in a further improvement in the agreement between measured and hindcast wave heights (Fig. 11, Table 4). One effect of refraction is to spread the wave energy entering the Gulf, resulting in lower heights for waves reaching Mangawhai. The bias in the wave height is reduced to +9 cm, and correlation increases to 0.93, and mean period is also slightly better predicted. Peak wave direction is reproduced satisfactorily, although this is an awkward statistic for comparison. Where mixed swell and wind-sea from different directions are present, peak direction values derived from both measurements and modelling can jump between separate peaks.

EFFECTS OF THE PROPAGATION SCHEME

As noted in connection with the hindcast representation of wave heights at Maui, we need to consider the role of the numerical scheme as a possible source of error for waves propagating past diagonal land boundaries.

Suppose $F_{i,j} = F(f,\theta,x_i,y_j,t)$ is a spectral component propagating at an angle θ to the x-axis, with $0 \quad \theta \quad \pi/2$ (Fig. 3). Then, ignoring all other processes, including great-circle propagation effects, the WAM first-order upwind scheme will propagate that component with an equation:

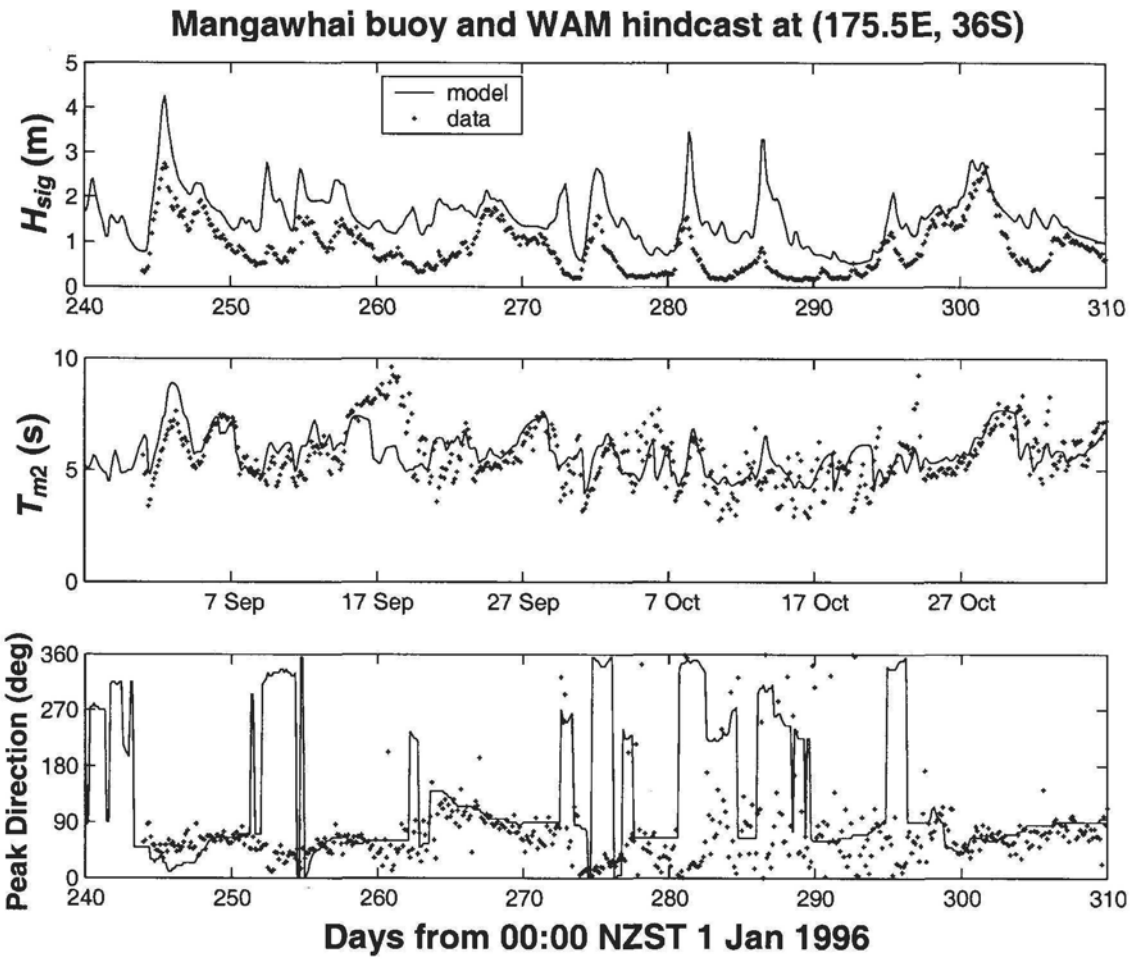

Fig. 9 Significant wave height, second-moment mean wave period, and peak wave direction, measured at the Mangawhai wave buoy, compared with the WAM model hindcast at the nearest cell of the 1.125° south-west Pacific grid. Nautical convention is used, i.e., the direction from which waves arrive is plotted, taken clockwise from North.

Table 4 Statistics from the comparison between hindcast and measured significant wave height H_{sig} and mean period T_{m2} at the Mangawhai buoy. Bias (model minus data) with 95% confidence limits, root-mean-square error (RMSE), scatter index (SI), and correlation (R) are listed. Separate comparisons are made for the deep-water WAM hindcast at the nearest model cell, filtered for limited fetch, and propagated shoreward by the nested SWAN model.

	H_{sig} model comparison				T_{m2} model comparison			
Method	Bias (m)	RMSE (m)	SI	R	Bias (s)	RMSE (s)	SI	R
WAM, nearest cell	0.74±0.05	0.85	0.99	0.74	0.17±0.13	1.16	0.21	0.52
WAM, filtered	0.27±0.05	0.38	0.51	0.91	0.97±0.13	1.66	0.30	0.41
SWAN, nested	0.09±0.05	0.22	0.26	0.93	−0.24±0.13	1.05	0.19	0.67

$$\frac{\partial F_{i,j}}{\partial t} + C_g \cos\theta \frac{1}{\Delta x}\left[F_{i,j} - F_{i-1,j}\right] + C_g \sin\theta \frac{1}{\Delta y}\left[F_{i,j} - F_{i,j-1}\right] = 0 \qquad (12)$$

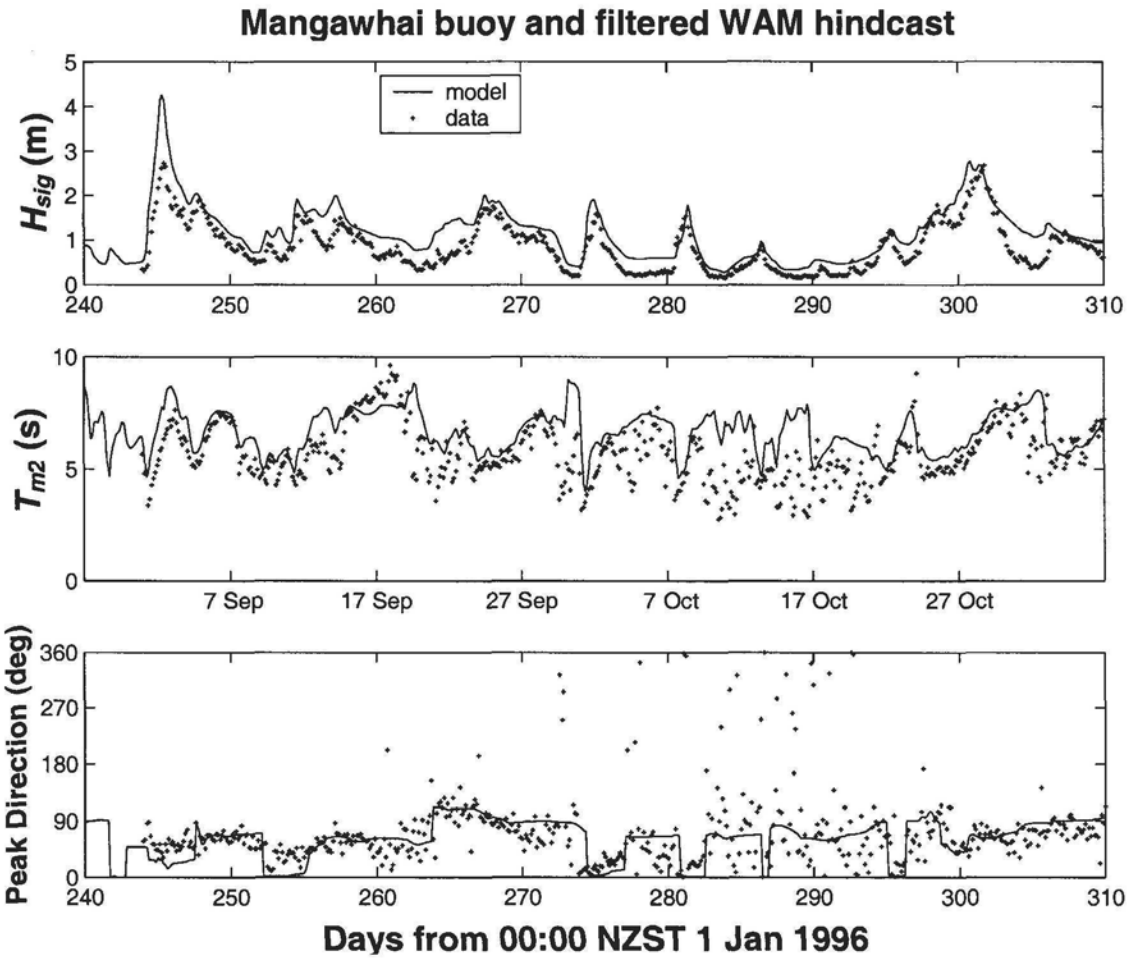

Fig. 10 Significant wave height, mean wave period, and peak wave direction measured at the Mangawhai wave buoy, compared with the WAM model hindcast filtered to adjust for limited fetch.

which, for steady state conditions, is solved by:

$$F_{i,j} = \lambda F_{i-1,j} + (1-\lambda)F_{i,j} \quad (13)$$

where:

$$\lambda = \frac{\Delta y \cos\theta}{\Delta y \cos\theta + \Delta x \sin\theta} \quad (14)$$

For diagonal propagation, the weight $\lambda \approx 0.5$ and a given cell receives energy from its western and southern neighbours with near-equal weighting. If the southern neighbour, for example, is land, then only the western contribution will be transmitted, reduced by the weighting factor λ. With successive steps along a diagonal coast, represented by a "saw-tooth" pattern of wet and dry cells, energy that ideally would be allowed to propagate freely will continue to be lost in this way.

The energy loss can be computed for a steady state, incident wave field by iterating Equation 13 in the down-wave direction. At Maui, the hindcast estimates that the waves predominantly arrive from the south-west (15% occurrence), west-south-west (41%), and west (20%) (Fig. 5). For a homogeneous wave field entering a rectangular region enclosing New Zealand from each of those directions, WAM's upwind propagation scheme transmits respectively 40%, 81%, and 100% of the energy to the grid cell nearest to the Maui site. If we estimate the fraction of the direction bins that have infinite fetch, as an alternative method of estimating transmission, we find 44%, 100%, and 100% respectively. So notably, the propagation scheme may be causing energy of waves travelling over long fetches from the dominant

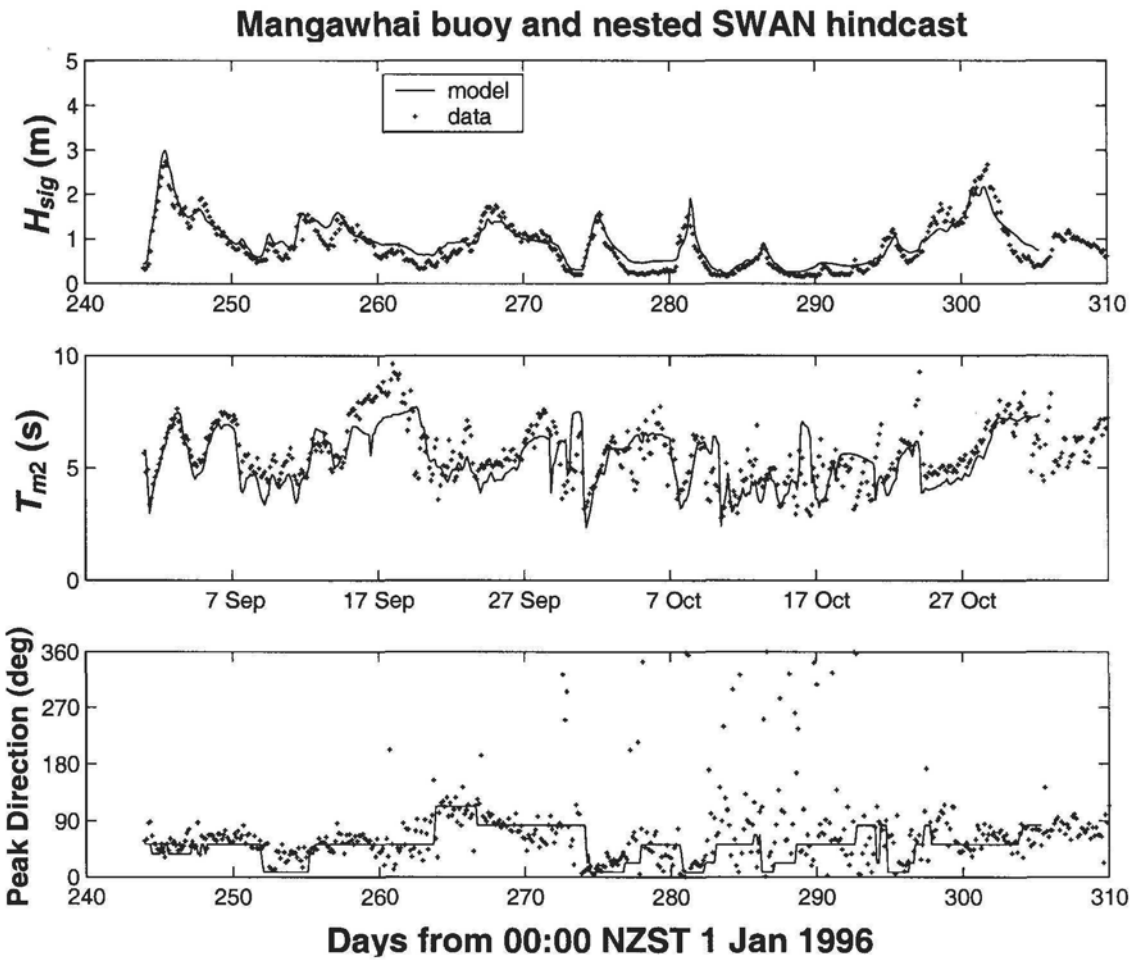

Fig. 11 Significant wave height, mean wave period, and peak wave direction measured at the Mangawhai wave buoy, compared with the results obtained using the SWAN model.

direction (west-south-west) to be underestimated by c. 20%, or wave heights by 10%. If we assume that the occurrence of mean direction approximates the typical directional spread of the energy density spectrum, and take a weighted average of this effect in all wave directions, this suggests a mean wave height underestimate of 4–5%.

Other locations will also be affected. At Hokitika, for the predominant west-south-west incident direction (54% occurrence), the combined propagation and up-fetch interpolation schemes transmit 75% of energy from the boundary. The other directions with significant occurrence are unaffected, as waves from the west are 100% propagated, whereas empirical fetch-limited spectral densities will be used for waves from the south-west. This suggests that correcting errors introduced by the propagation scheme will increase the hindcast mean wave height by c. 7%, making the same assumptions as above. Unfortunately this would compound the observed overprediction of measured heights. At Baring Head, the combined numerical scheme correctly gives 100% transmission for wave energy from the south and south-south-east, but only 41% transmission for energy from the south-south-west sector (33% occurrence), which has fully open fetches.

The exact influence of this excess absorption of energy is difficult to estimate for realistic inhomogeneous wave fields, where swell propagating long distances will be mixed with waves generated over shorter fetches. This can only be adequately tested

by repeating the simulation with a revised propagation scheme, such as that employed by the WAVEWATCH model (Tolman 1991), which uses an up-fetch interpolation scheme for propagation near land boundaries.

CONCLUSIONS

A wave model has been implemented to simulate wave generation in the oceans around New Zealand, and applied to produce a long-term hindcast that provides synthetic regional wave climate information. We have sought to validate the hindcast against nearshore data from a set of buoy deployments representative of the various wave climates found around the New Zealand coast. To make this comparison, we have used two principal methods to derive inshore wave spectra from those simulated offshore by the WAM model.

The first of these involves interpolation of the spectrum from up-fetch grid cells, and correcting for limited fetch. This is intended for use where wave conditions are affected by the nearby coastline, but where the water is sufficiently deep for refraction effects to be insignificant. With this adjustment, we find that the hindcast provides a satisfactory representation of wave conditions for most parts of the New Zealand coast that are predominantly exposed to deep-water wave conditions. Regression between measured and hindcast significant heights at the four deep-water sites (100–120 m depth) achieved correlation coefficients averaging 0.82, and scatter indices (RMS error/mean) averaging 0.28 (Table 2). The primary determinant of the quality of such a wave simulation is the accuracy of the wind fields driving it, so this result reflects positively on the quality of the ECMWF reanalysis data set, as much as on the WAM model.

One limitation that has been identified though, is in the excessive dissipation by the WAM upwind propagation scheme of wave energy propagating near parallel to a diagonal coast. This is particularly relevant to modelling the New Zealand region, given the orientation of the North and South Islands to waves from the south-west that constitute a major component of the regional wave climate. A simple way to alleviate this problem is to select a grid locally aligned with the main islands, as has been done in previous (second-generation) modelling studies of the region (Laing 1992, 1993). This is not, however, convenient to implement with WAM, which is designed to be used on a latitude/longitude grid for large-scale applications. A more satisfactory modification would be the inclusion of a land-sea boundary treatment similar to that of Tolman (1991).

The quality of agreement of the filtered hindcast and buoy data is also reduced at some of the shallower sites, where refraction effects become significant. In comparisons of hindcast and measured significant wave heights at the four shallower sites (30–45 m depth), the average correlation coefficient and scatter index were 0.75 and 0.49 respectively (Table 2).

Where the bathymetry is complex, refraction effects can best be addressed by using high resolution modelling on a nested grid. The use of the SWAN nearshore spectral model to provide a transformation from deep-water hindcast spectra to shallow water has been tested in the outer Hauraki Gulf. This approach was found to allow a considerably better agreement with buoy data at the Mangawhai site than is provided by interpolation and fetch-limited correction of deep-water hindcast spectra. Some limitations do, however, remain in this approach. The relatively slow computation times make it more suitable for short wave records than for application to long-term hindcasts over many years. Also, although wave generation by local winds can be readily included in the SWAN simulation, this was not done for the present study. For the Mangawhai site, located close to shore but reasonably exposed to oceanic swell, waves produced by offshore winds should make a minimal contribution, but elsewhere in the Hauraki Gulf, or a similar water body, this may not apply. Ideally, a local wind field should be applied that is consistent with the winds used in the deep-water hindcast, but also reflecting the effects of topography in modifying wind speed and direction.

The coastal wave climate derived from this hindcast is dominated by waves arriving from the south-west quadrant, often generated in the Southern Ocean. This is observed at all parts of the coast exposed to this quadrant, and there is a clear progression of both wave heights and periods decreasing from south-west to north-east, related to the degree of this exposure. This is consistent with the patterns observed in previous studies using buoy data (Pickrill & Mitchell 1979), modelling (Laing 1993), and satellite data (Laing 2000; Laing & Gorman 2000). On the north-east coast of the North Island, which is not exposed to these south-westerly swells, and the south-east coast, which is only partly exposed, a broader directional distribution is seen.

Comparison with available wave records has indicated that a degree of confidence can be placed

in wave climatology derived from the hindcast, as well as pointing out aspects of the modelling procedure that merit further attention. It can now be expected that the availability of hindcast information will go a long way towards filling the gaps in the wave climate information needed for a wide range of applications on the New Zealand coast.

ACKNOWLEDGMENTS

This work was carried out with support from the Public Good Science Fund (Contract No. C01X0115) of the Foundation for Research, Science and Technology. The various buoy deployments were carried out or supported by BTW Associates, University of Auckland, Shell-BP Todd Oil Services, Ministry of Works and Development, Environment Canterbury, Christchurch City Council, TranzRail, and Auckland Regional Council, all of whom we acknowledge for making data available. We thank present and past NIWA staff members Graham Macky, Malcolm Greig, Geoff Latimer, Sandra Kingsland, Jeremy Walsh, and Warren Thompson for assistance in gathering and providing wave data. The authors thank the reviewers for the helpful comments they provided.

REFERENCES

Babanin, A. V.; Soloviev, Y. P. 1998: Field investigation of transformation of the wind wave frequency spectrum with fetch and the stage of development. *Journal of Physical Oceanography 28*: 563–576.

Black, K. P.; Bell, R. G.; Oldman, J. W.; Carter, G. S.; Hume, T. M. 2000: Features of the 3-dimensional barotropic and baroclinic circulation in the Hauraki Gulf, New Zealand. *New Zealand Journal of Marine and Freshwater Research 34*: 1–28.

Booij, N.; Ris, R. C.; Holthuijsen, L. H. 1999: A third-generation wave model for coastal regions 1. Model description and validation. *Journal of Geophysical Research 104*: 7649–7666.

Cox, A. T.; Swail, V. R. 2001: A global wave hindcast over the period 1958–1997: Validation and climate assessment. *Journal of Geophysical Research 106*: 2313–2329.

Ewans, K. C. 1998: Observations of the directional spectrum of fetch-limited waves. *Journal of Physical Oceanography 28*: 495–512.

Ewans, K. C.; Kibblewhite, A. C. 1990: An examination of fetch-limited waves off the West Coast of New Zealand by a comparison with the JONSWAP results. *Journal of Physical Oceanography 20*: 1278–1296.

Gibson, J. K.; Kållberg, P.; Uppala, S.; Hernandez, A.; Nomura, A.; Serrano, E. 1999: ERA–15 Description. European Centre for Medium-Range Weather Forecasts. ECMWF Re-Analysis Project Report Series 1.

Gillbanks, R. J. 1989: Chart NZ55 Cape Runaway to Table Cape. Hydrographic Office, Royal New Zealand Navy.

Gorman, R. M.; Bryan, K. R.; Laing, A. K. 2003: Wave hindcast for the New Zealand region: deep-water wave climate. *New Zealand Journal of Marine and Freshwater Research 37*: 589–612.

Gorman, R. M.; Laing, A. K. 2001: Bringing wave hindcasts to the New Zealand coast. *Journal of Coastal Research Special Issue 34 (ICS 2000 New Zealand)*: 30–37.

Greig, M. J.; Proctor, R. 1988: A numerical model of the Hauraki Gulf, New Zealand. *New Zealand Journal of Marine and Freshwater Research 22*: 379–390.

Günther, H.; Rosenthal, W.; Stawarz, M.; Carretero, J. C.; Gomez, M.; Lozano, I.; Serano, O.; Reistad, M. 1998: The wave climate of the north-east Atlantic over the period 1955–1994: The WASA wave hindcast. *Global Atmosphere and Ocean System 6*: 121–163.

Harris, T. F. W. 1990: Greater Cook Strait—form and flow. New Zealand Oceanographic Institute, DSIR Marine & Freshwater, Wellington, New Zealand.

Hasselmann, K. 1974: On the spectral dissipation of ocean waves due to whitecapping. *Boundary Layer Meteorology 6*: 107–127.

Hasselmann, K.; Barnett, T. P.; Bouws, E.; Carlson, H.; Cartwright, D. E.; Enke, K.; Ewing, J. A.; Gienapp, H.; Hasselmann, D. E.; Kruseman, P.; Meerburg, A.; Müller, P.; Olbers, D. J.; Richter, K.; Sell, W.; Walden, H. 1973: Measurements of wind-wave growth and swell decay during the Joint North Sea Wave Project (JONSWAP). *Deutsche Hydrographische Zeitschrift. Supplement A8*: 1–95.

Hasselmann, S.; Hasselmann, K.; Bauer, E.; Bertotti, L.; Cardone, C. V.; Ewing, J. A.; Greenwood, J. A.; Guillaume, A.; Janssen, P. A. E. M.; Komen, G. J.; Lionello, P.; Reistad, M.; Zambresky, L. 1988: The WAM Model—a third generation ocean wave prediction model. *Journal of Physical Oceanography 18*: 1775–1810.

Hasselmann, S.; Ross, D. B.; Müller, P.; Sell, W. 1976: A parametric wave prediction model. *Journal of Physical Oceanography 6*: 200–228.

Holthuijsen, L. H.; Booij, N.; Herbers, T. H. C. 1989: A prediction model for stationary, short-crested waves in shallow water with ambient currents. *Coastal Engineering 13*: 23–54.

Holthuijsen, L. H.; Booij, N.; Ris, R. C. 1993: A spectral wave model for the coastal zone. Proceedings of the 2nd International Symposium on Ocean Wave Measurement and Analysis, New Orleans. Pp. 630–641.

Kibblewhite, A. C.; Bergquist, P. R.; Foster, B. A.; Gregory, M. R.; Miller, M. C. 1982: Maui Development Environmental Study. Report on Phase Two 1977–1981. Prepared by the University of Auckland for Shell BP and Todd Oil Services Limited. Auckland, October 1982.

Komen, G. J.; Hasselmann, S.; Hasselmann, K. 1984: On the existence of a fully developed windsea spectrum. *Journal of Physical Oceanography 14*: 1271–1285.

Laing, A. K. 1992: A spectral model for the sea-state with explicit forcing terms. *Applied Ocean Research 14*: 341–351.

Laing, A. K. 1993: Estimates of wave height data for New Zealand waters by numerical modelling. *New Zealand Journal of Marine and Freshwater Research 27*: 157–175.

Laing, A. K. 2000: New Zealand wave climate from satellite observations. *New Zealand Journal of Marine and Freshwater Research 34*: 727–744.

Laing, A. K. 2001: Rapid growth of waves on the east coast of New Zealand. *Journal of Coastal Research Special Issue 34 (ICS 2000 New Zealand)*: 38–44.

Laing, A. K.; Gorman, R. M. 2000: The ocean wave climate around New Zealand from satellites and modelling. *Water and Atmosphere 8*: 20–23.

Macky, G. H.; Latimer, G. J.; Smith, R. K. 1995: Wave climate of the Western Bay of Plenty, New Zealand, 1991–93. *New Zealand Journal of Marine and Freshwater Research 29*: 311–327.

NOAA 1988: Digital relief of the surface of the Earth. NOAA, National Geophysical Data Center. Data Announcement 88-MGG-02.

Pickrill, R. A.; Mitchell, J. S. 1979: Ocean wave characteristics around New Zealand. *New Zealand Journal of Marine and Freshwater Research 13*: 501–552.

Ris, R. C.; Holthuijsen, L. H.; Booij, N. 1994: A spectral model for waves in the near shore zone. Proceedings of the 24th Conference on Coastal Engineering, Kobe, Japan. Pp. 68–78.

Ris, R. C.; Holthuijsen, L. H.; Booij, N. 1999: A third-generation wave model for coastal regions 2. Verification. *Journal of Geophysical Research 104*: 7667–7681.

Stanton, B. R. 1992: New Zealand ocean wave data inventory. *New Zealand Journal of Marine and Freshwater Research 26*: 175–178.

Stanton, B. R. 1998: Ocean surface winds off the west coast of New Zealand: a comparison of ocean buoy, ECMWF model, and land-based data. *Journal of Atmospheric and Oceanic Technology 15*: 1164–1170.

Sterl, A.; Komen, G. J.; Cotton, P. D. 1998: Fifteen years of global wave hindcasts using winds from the European Centre for Medium-Range Weather Forecasts reanalysis: validating the reanalyzed winds and assessing the wave climate. *Journal of Geophysical Research 103*: 5477–5492.

Tolman, H. L. 1991: A third-generation model for wind waves on slowly varying, unsteady, and inhomogeneous depths and currents. *Journal of Physical Oceanography 21*: 782–797.

Walsh, J. 2001: Canterbury directional wave buoy quarterly report—November 2000–January 2001. NIWA, Client Report CHC01/31.

Walsh, J.; Mason, C. 2000: Canterbury directional wave buoy quarterly report—September 1999–October 2000. NIWA, Client Report CHC00/99.

Yuan, X. 2002: High wind distribution in the Southern Ocean. Eos Transactions. *American Geophysical Union Western Pacific Geophysics Meeting Supplement 83*: Abstract OS51B–09.

(*Appendix 1 overleaf*)

Appendix 1 Definition of wave statistics.

From the directional spectrum $F(f,\theta)$, a one-dimensional spectrum can be obtained by integrating over propagation directions:

$$S(f) = \int_0^{2\pi} F(f,\theta)d\theta \tag{A1}$$

From this, spectral moments

$$M_j = \int_0^{\infty} df\ f^j S(f) \tag{A2}$$

are computed for integer values of j, allowing spectral wave statistics to be defined, including significant height, mean frequency, and first- and second-moment mean periods, respectively:

$$H_{sig} = 4\sqrt{M_0} \tag{A3}$$

$$f_{mean} = 1/T_{m1} = M_1/M_0 \tag{A4}$$

$$T_{m2} = \sqrt{M_0/M_2} \tag{A5}$$

The latter is often similar to the quantity T_z obtained from zero downcrossing analysis.
A measure of mean direction:

$$\theta_{mean} = \arctan\left(\frac{S_0}{C_0}\right) \tag{A6}$$

can also be derived using directional moments

$$C_0 = \int_0^{\infty} df \int_0^{2\pi} d\theta\ F(f,\theta)\cos\theta \tag{A7}$$

$$S_0 = \int_0^{\infty} df \int_0^{2\pi} d\theta\ F(f,\theta)\sin\theta \tag{A8}$$

The results are presented as the direction to which waves propagate, in degrees clockwise from north.
In comparisons between time series of measurements $\{x_i = x(t_i) : i = 1,...,N\}$ and hindcast values $\{y_i = y(t_i) : i = 1,...,N\}$, the root-mean-square error (RMSE) and the correlation R are defined as:

$$\mathrm{RMSE} = \sqrt{\frac{1}{N}\sum_{i=1}^{N}(y_i - x_i)^2} \tag{A9}$$

$$R = \frac{\sum_{i=1}^{N}(x_i - \bar{x})(y_i - \bar{y})}{\sqrt{\sum_{i=1}^{N}(x_i - \bar{x})^2 \sum_{i=1}^{N}(y_i - \bar{y})^2}} \tag{A10}$$

respectively, where $\bar{x}$ and $\bar{y}$ are the respective means.